International Journal of Science and Engineering Applications
Volume 4 Issue 2, 2015, ISSN-2319-7560 (Online)

Influence of Titanium Oxide on Creep Behavior, Microstructure and Physical Properties of Tin-Antimony and Tin-Aluminum-Antimony Based Bearing Alloys

Abu Bakr El- Bediwi
Metal Physics Lab., Physics Department, Faculty of Science, Mansoura University
Mansoura, Egypt

Maison Hamid Grayb
Ministry of education
Iraq

Mustafa Kamal
Metal Physics Lab., Physics Department, Faculty of Science, Mansoura University
Mansoura, Egypt

Abstract: Influence of adding titanium oxide (TiO_2) nanoparticles on creep behavior, structure, mechanical and thermal properties of tin-antimony-lead and tin-aluminum-antimony bearing alloys have been studied and analyzed. Stress exponent of tin- antimony- lead and tin-aluminum- antimony- lead alloys decreased after adding titanium oxide. Elastic modulus of tin- antimony- lead increased after adding titanium oxide. Internal fiction of tin- antimony- lead and tin- aluminum- antimony- lead alloys varied after adding titanium oxide. Microstructure of tin-antimony- lead and tin- aluminum- antimony- lead alloys changed after adding titanium oxide. Strengths of tin- antimony- lead and tin- aluminum-antimony- lead alloys increased after adding titanium oxide. Thermal parameters of tin- antimony- lead and tin- aluminum- antimony- lead alloys varied after adding titanium oxide. The $Sn_{79}Sb_{15}Pb_5(TiO_2)_1$ alloy has better bearing properties such as lowest internal friction, high elastic modulus and higher thermal diffusivity for industrial applications
.

Key words: stress exponent, titanium oxide, bearing alloys, internal fiction, creep indentation, thermal properties, mechanical properties

1. INTRODUCTION

Bearing is a device to allow constrained relative motion between two or more parts, typically rotation or linear movement. Bearing is a device used to transmit loads between relatively moving surfaces. The tribological properties of tin-based bearing alloys with different compositions, (7% and 20%), have been investigated [1]. Structure, electrical resistivity and elastic modulus of $SnSb_7X$ (X = 0, Cu, Ag, or Cu and Ag) and $Pb_{63-x}Sn_{30}Sb_7Cu_x$ [x=0 or x≤2.5] alloys have been studied and analyzed [2, 3]. Electrical resistivity, elastic modulus and internal friction of $Pb_{63}Sn_{30}Sb_7$ decreases after adding Cu. Mechanical properties of Sn-Sb bearing alloy have been evaluated [4]. Mechanical properties of Sn-Sb improved after adding 1 wt. % of Cu or Ag. Also the elastic modulus, internal friction and stiffness of Sn-Sb based bearing alloys varied after annealing for 2 and 4 h at 120, 140 and 160 °C. Creep behavior of $SnSb_5$ alloy and $SnPb40Sb_{2.5}$ peritectic alloy were studied by long time Vickers indentation testing at room temperature [5- 7]. Increasing Sb content from 7.5% to 20% provided an increase in hardness. Tensile properties of $SnSb_5Bi_{1.5}$ and $SnSb_5Cu_{1.5}$ alloys have been studied at different strain rates ranging from 5×10^{-4} to 1×10^{-2} s^{-1} over the wide temperature range of 298-400 K [8]. Strength and ductility of $SnSb_5$ improved after adding Bi and Cu. Creep behavior, elastic modulus and internal friction of $SnSb_{10}Cu_2X_2$ (X = Pb, Ag, Se, Cd and Zn) alloys have been investigated and stress exponents have been determined [9]. The effect of solidification rate, heating and micro additions on microstructure and hardness of tin-based white metals have been studied [10, 11]. Rapid cooling suppresses formation and growth of SbSn cuboids and increases hardness. Structure, hardness, mechanical and electrical transport properties of $Sn_{90-x}Sb_{10}Bi_x$ (x = 0, or x ≥1) alloys have been studied and analyzed [12]. Electrical resistivity and hardness of $SnSb_{10}$ increased after adding bismuth content. Internal friction, elastic modulus and thermal diffusivity of $SnSb_{10}$ decreased after adding bismuth content. The effects of small amounts of Ag and Cu on the as-cast microstructure and creep properties of the $SnSb_5$ alloy have been investigated [13]. Small additions of Ag and Cu elements could effectively change the creep behavior of the $SnSb_5$ alloy. The friction coefficients of

$SnSb_{20.2}Pb_{16.6}Cu_{2.6}$ is lower than that of $SnSb_{7.2}Pb_{0.4}Cu_3$ under all scratch test conditions [14]. The directionally solidified microstructure of $SnSb_{16}$ hyperperitectic alloy has been investigated at various solidification rates using a high-thermal gradient directional solidification apparatus [15]. The volume fraction of the SnSb phase firstly decreased and then increased when the solidification rate increased. The aim of this work was to study and analyze the effects of adding titanium oxide nanoparticles on creep behavior, structure, mechanical and thermal properties of tin-antimony-lead and tin-aluminum-antimony based alloys.

2. EXPERIMENTAL WORK

Two groups of alloys, $Sn_{80-x}Sb_{15}Pb_5(TiO_2)_x$ (x= 0.5, 1 and 1.5 wt.%) and $Sn_{60-x}Al_{20}Sb_{15}Pb_5(TiO_2)_x$ (x= 0.5, 1 and 1.5 wt.%), were molten in the muffle furnace. Using elements tin, antimony, lead, aluminum and titanium oxide have a high purity, more than 99.95%. The resulting ingots were turned and re-melted several times to increase the homogeneity of the ingots. From these ingots, long ribbons of about 3-5 mm width and ~ 70 µm thickness were prepared as the test samples by directing a stream of molten alloy onto the outer surface of rapidly revolving copper roller with surface velocity 31 m/s giving a cooling rate of 3.7×10^5 k/s. The samples then cut into convenient shape for the measurements using double knife cuter. Structure of used alloys was performed using an Shimadzu x–ray diffractometer (Dx–30, Japan) of Cu–Kα radiation with λ=1.54056 Å at 45 kV and 35 mA and Ni–filter in the angular range 2θ ranging from 0 to 100° in continuous mode with a scan speed 5 deg/min. Scanning electron microscope JEOL JSM-6510LV, Japan was used to study microstructure of used samples. The melting endotherms of used alloys were obtained using a SDT Q600 V20.9 Build 20 instrument.

A digital Vickers micro-hardness tester, (Model-FM-7- Japan), was used to measure Vickers hardness values of used alloys. Internal friction Q^{-1} and the elastic constants of used alloys were determined using the dynamic resonance method [16-18].

3. RESULTS AND DISCUSSIONS

Structure

X-ray diffraction patterns of $Sn_{80-x}Sb_{15}Pb_5(TiO_2)_x$ (x= 0.5, 1 and 1.5 wt.%) rapidly solidified alloys have lines corresponding to β-Sn, Pb, Sb and SbSn intermetallic phases as shown in Figure 1. X-ray analysis of $Sn_{80}Sb_{15}Pb_5$ show that, formed phases (intensity, peak broadness, miller indices, position (2θ), and area under peaks) changed after adding of $(TiO_2)_x$. That is because TiO_2 disappeared, dissolved in the matrix of alloy. Also crystal particle size of β- Sn in $Sn_{80}Sb_{15}Pb_5$ alloy increased after adding TiO_2 as seen in Table 1.

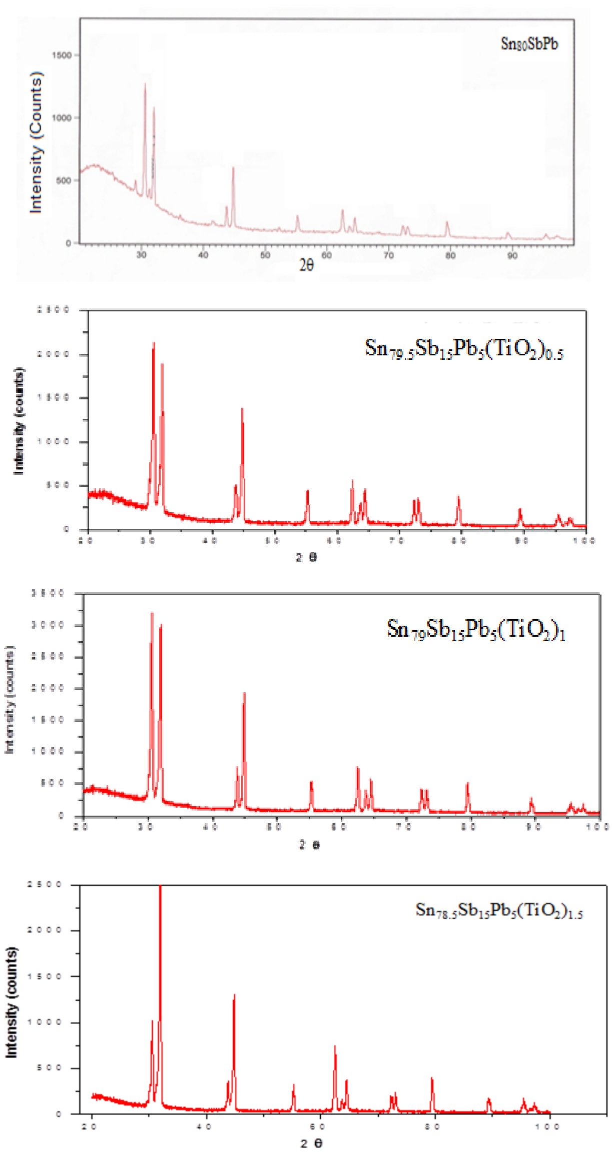

Figure 1:- x-ray diffraction patterns of $Sn_{80-x}Sb_{10}Pb_5(TiO_2)_x$ alloys

Table 1:- crystal particle size of β- Sn in $Sn_{80-x}Sb_{10}Pb_5(TiO_2)_x$ alloys

Samples	Particle size Å
$Sn_{80}Sb_{15}Pb_5$	317.25
$Sn_{79.5}Sb_{15}Pb_5(TiO_2)_{0.5}$	395.12
$Sn_{79}Sb_{15}Pb_5(TiO_2)_1$	448.06
$Sn_{78.5}Sb_{15}Pb_5(TiO_2)_{1.5}$	415.38

Scanning electron micrographs, SEM, of $Sn_{80-x}Sb_{15}Pb_5(TiO_2)_x$ alloys show heterogeneous structure as shown in Figure 2 and that agreed with x-ray analysis. Adding TiO_2 caused change in microstructure of $Sn_{80}Sb_{15}Pb_5$ alloy.

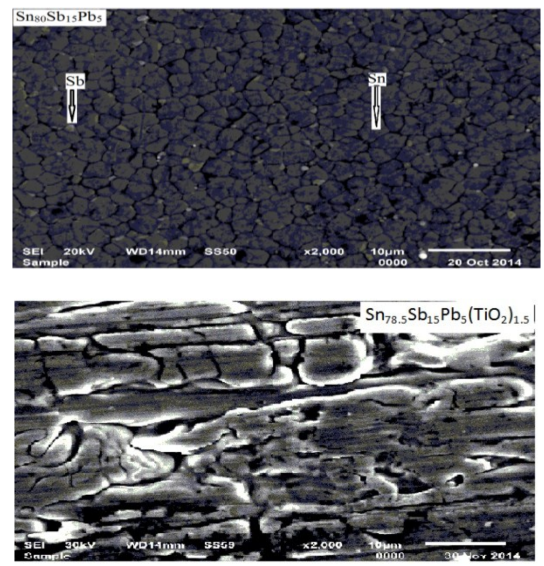

Figure 2:- SEM of $Sn_{80-x}Sb_{10}Pb_5(TiO_2)_x$ alloys

X-ray diffraction patterns of $Sn_{60-x}Al_{20}Sb_{15}Pb_5(TiO_2)_x$ (x= 0.5, 1 and 1.5 wt.%) rapidly solidified alloys have lines corresponding to β- Sn, Pb, Sb and SbSn intermetallic phases as shown in Figure 3. X-ray analysis of $Sn_{60}Al_{20}Sb_{15}Pb_5$ show that, formed phases (intensity, peak broadness, miller indices, position (2θ), and area under peaks) changed after adding of $(TiO_2)_x$. That is because Al and TiO_2 disappeared\ or not detected, dissolved in the matrix of alloy. Also crystal particle size of β- Sn in $Sn_{60}Al_{20}Sb_{15}Pb_5$ alloy increased after adding TiO_2 as seen in Table 2.

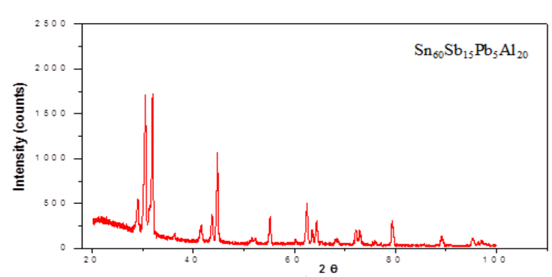

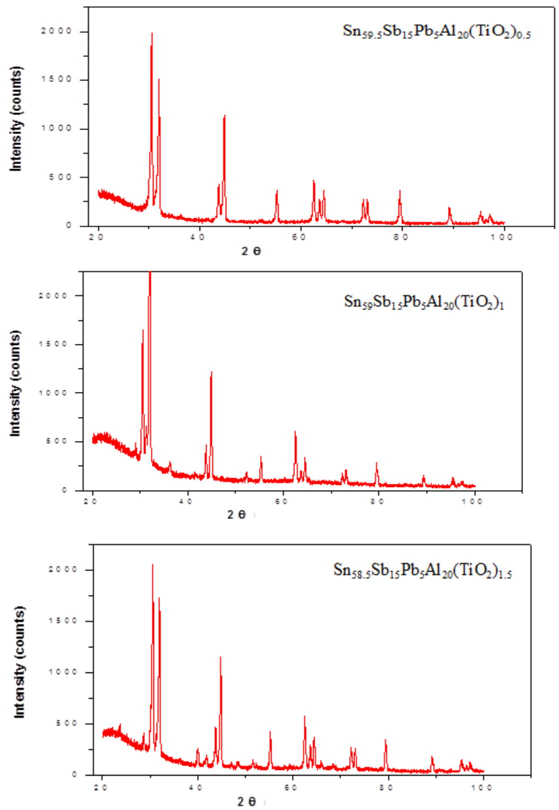

Figure 3:- x-ray diffraction patterns of Sn_{60-x} $Al_{20}Sb_{15}Pb_5$ $(TiO_2)_x$ alloys

Table 2:- crystal particle size of β- Sn in Sn_{60-x} $Al_{20}Sb_{15}Pb_5(TiO_2)_x$ alloys

Samples	Particle size Å
Sn_{60} $Al_{20}Sb_{15}Pb_5$	337.70
$Sn_{59.5}$ $Al_{20}Sb_{15}Pb_5(TiO_2)_{0.5}$	412.47
Sn_{59} $Al_{20}Sb_{15}Pb_5(TiO_2)_1$	409.78
$Sn_{58.5}$ $Al_{20}Sb_{15}Pb_5(TiO_2)_{1.5}$	368.36

Scanning electron micrographs, SEM, of $Sn_{60-x}Al_{20}Sb_{15}Pb_5(TiO_2)_x$ alloys show heterogeneous structure as shown in Figure 4 and that agreed with x-ray analysis.

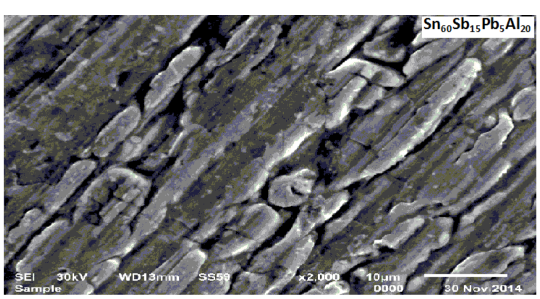

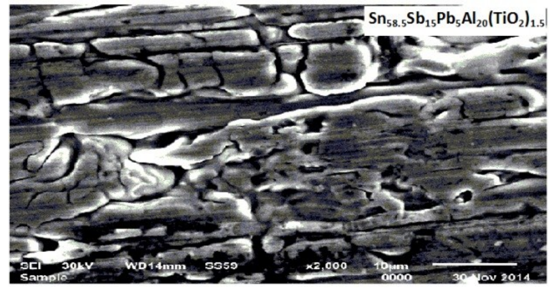

Figure 4:- SEM of Sn_{60-x} $Al_{20}Sb_{15}Pb_5(TiO_2)_x$ alloys

Mechanical properties

The elastic constants are directly related to atomic bonding and structure. Elastic modului of $Sn_{80-x}Sb_{10}Pb_5(TiO_2)_x$ alloys are listed in Table 3. Elastic modulus of $Sn_{80}Sb_{15}Pb_5$ alloy increased after adding TiO_2 nanoparticles.

The resonance curves of $Sn_{80-x}Sb_{10}Pb_5(TiO_2)_x$ alloys are shown in Figure 5. Calculated internal friction and thermal diffusivity of $Sn_{80-x}Sb_{10}Pb_5(TiO_2)_x$ alloys are listed in Table 3. Internal friction of $Sn_{87}Sb_{10}Pb_3$ alloy varied after adding TiO_2 nanoparticles.
The $Sn_{79}Sb_{15}Pb_5(TiO_2)_1$ alloy has better bearing properties such as lowest internal friction, high elastic modulus and higher thermal diffusivity for industrial applications.

Table 3:- elastic modului, internal friction and thermal diffusivity of $Sn_{80-x}Sb_{10}Pb_5(TiO_2)_x$ alloys

Samples	E GPa	μ GPa	B GPa	Q^{-1}	D_{th} x10^{-8} m^2\sec
$Sn_{80}Sb_{15}Pb_5$	24.28	8.93	28.80	0.034	21.12
$Sn_{79.5}Sb_{15}Pb_5(TiO_2)_{0.5}$	32.96	12.18	37.49	0.036	17.7
$Sn_{79}Sb_{15}Pb_5(TiO_2)_1$	38.25	14.08	45.09	0.029	34.5
$Sn_{78.5}Sb_{15}Pb_5(TiO_2)_{1.5}$	42.67	15.71	50.12	0.041	12.3

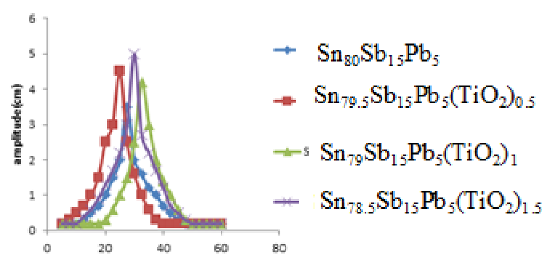

Figure 5:- resonance curves of $Sn_{80-x}Sb_{10}Pb_5(TiO_2)_x$ alloys

Elastic modului of $Sn_{60-x}Al_{20}Sb_{15}Pb_5(TiO_2)_x$ alloys are listed in Table 4. Elastic modulus of Sn_{60} $Al_{20}Sb_{15}Pb_5$ alloy varied after adding TiO_2 nanoparticles.

The resonance curves of $Sn_{60-x}Al_{20}Sb_{15}Pb_5(TiO_2)_x$ alloys are shown in Figure 6. Calculated internal friction and thermal diffusivity of $Sn_{60-x}Al_{20}Sb_{15}Pb_5(TiO_2)_x$ alloys are listed in Table 4. Internal friction of Sn_{60} $Al_{20}Sb_{15}Pb_5$ alloy varied after adding TiO_2 nanoparticles.

The Sn_{59} $Al_{20}Sb_{15}Pb_5(TiO_2)_1$ alloy has better bearing properties such as adequate internal friction, high elastic modulus and higher thermal diffusivity for industrial applications.

Table 4:- elastic modului, internal friction and thermal diffusivity of $Sn_{60-x}Al_{20}Sb_{15}Pb_5(TiO_2)_x$ alloys

Samples	E GPa	μ GPa	B GPa	Q^{-1}	D_{th} x10^{-8} m^2\sec
Sn_{60} $Al_{20}Sb_{15}Pb_5$	38.95	14.35	45.56	0.031	12.1
$Sn_{59.5}Al_{20}Sb_{15}Pb_5(TiO_2)_{0.5}$	36.99	13.63	43.11	0.033	16
Sn_{59} $Al_{20}Sb_{15}Pb_5(TiO_2)_1$	42.22	15.56	49.07	0.036	18.5
$Sn_{58.5}$ $Al_{20}Sb_{15}Pb_5(TiO_2)_{1.5}$	37.55	13.85	43.49	0.030	13.6

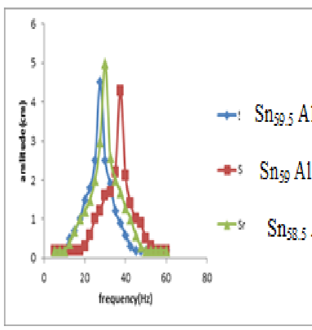

Figure 6:- resonance curves of $Sn_{60-x}Al_{20}Sb_{15}Pb_5(TiO_2)_x$ alloys

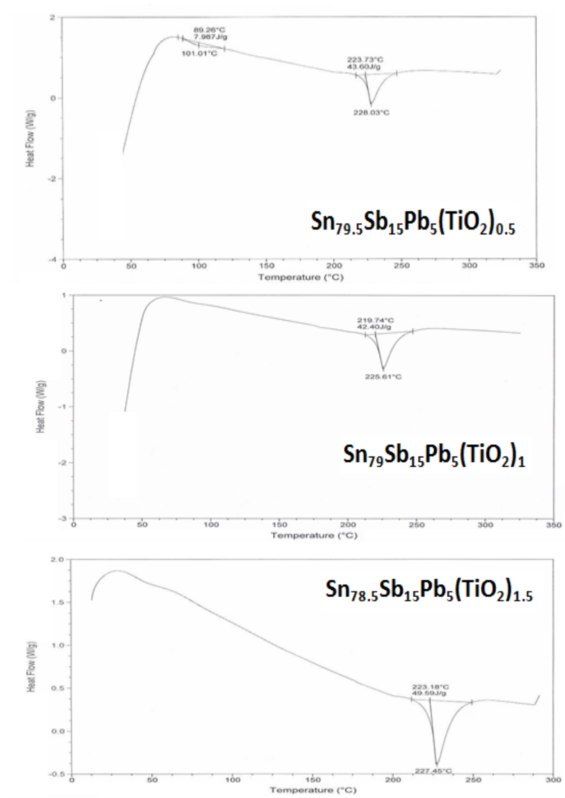

Figure 7:- DSC of $Sn_{87-x}Sb_{10}Pb_3(TiO_2)_x$ alloys

Thermal properties

Thermal analysis is often used to study solid state transformations as well as solid-liquid reactions. Figure 7 shows DSC thermographs for $Sn_{80-x}Sb_{10}Pb_5(TiO_2)_x$ alloys. Variation occurred in exothermal peak of $Sn_{80}Sb_{10}Pb_5$ alloy. The melting temperature and other thermal properties of $Sn_{80-x}Sb_{10}Pb_5(TiO_2)_x$ alloys are listed in Table 5. Melting temperature of $Sn_{80}Sb_{10}Pb_5$ alloy decreased after adding TiO_2 nanoparticles.

Specific heat, enthalpy and thermal conductivity of $Sn_{80}Sb_{10}Pb_5$ alloy varied after adding TiO_2 nanoparticles. That is because TiO_2 nanoparticles due change in matrix microstructure of $Sn_{80}Sb_{10}Pb_5$ alloy.

Table 5:- melting point and other thermal properties of $Sn_{80-x}Sb_{10}Pb_5(TiO_2)_x$ alloys

Samples	Melting point ºC	C_P J/g. ºC	Δ S J/g. ºC	K W.m^{-1}.K^{-1}
$Sn_{80}Sb_{15}Pb_5$	231.23	0.12	1.57	1.65
$Sn_{79.5}Sb_{15}Pb_5(TiO_2)_{0.5}$	228.03	3.41	0.189	1.86
$Sn_{79}Sb_{15}Pb_5(TiO_2)_1$	225.61	2.53	0.185	1.46
$Sn_{78.5}Sb_{15}Pb_5(TiO_2)_{1.5}$	227.45	3.35	0.215	2.77

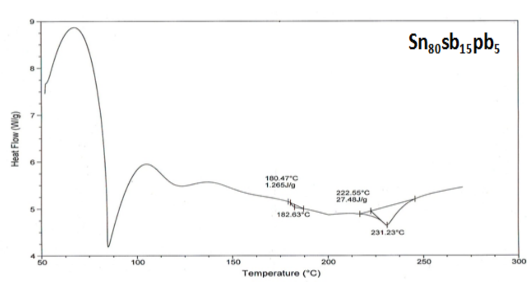

Figure 8 shows DSC thermographs for $Sn_{60-x}Al_{20}Sb_{15}Pb_5(TiO_2)_x$ alloys. Variation occurred in exothermal peak of Sn_{60} $Al_{20}Sb_{15}Pb_5$ alloy. The melting temperature and other thermal properties of $Sn_{60-x}Al_{20}Sb_{15}Pb_5(TiO_2)_x$ alloys are listed in Table 7. Melting temperature of Sn_{60} $Al_{20}Sb_{15}Pb_5$ alloy varied after adding TiO_2 nanoparticles.

Specific heat, enthalpy and thermal conductivity of $Sn_{80}Sb_{10}Pb_5$ alloy varied after adding TiO_2 nanoparticles. That is because TiO_2 nanoparticles due change in matrix microstructure of Sn_{60} $Al_{20}Sb_{15}Pb_5$ alloy.

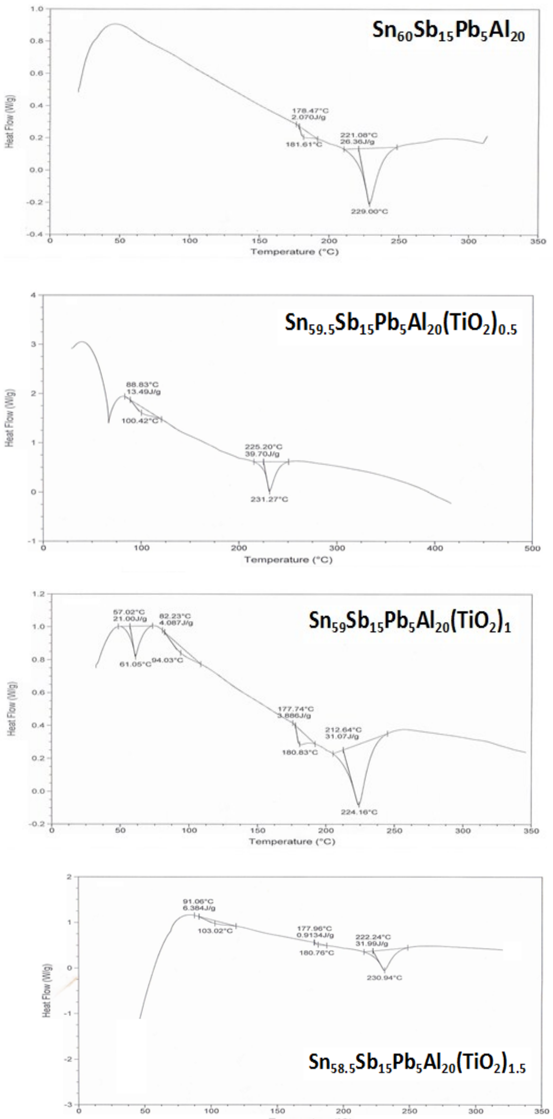

Figure 8:- DSC of $Sn_{60-x}Al_{20}Sb_{15}Pb_5(TiO_2)_x$ alloys

Table 6:- melting point and other thermal properties of $Sn_{60-x}Al_{20}Sb_{15}Pb_5(TiO_2)_x$ alloys

Samples	Melting point ºC	C_P J/g. ºC	Δ S J/g. ºC	K $W.m^{-1}.K^{-1}$
$Sn_{60}Al_{20}Sb_{15}Pb_5$	229	1.6	0.11	2.08
$Sn_{59.5}Al_{20}Sb_{15}Pb_5(TiO_2)_{0.5}$	231.27	2.46	0.18	2.28
$Sn_{59}Al_{20}Sb_{15}Pb_5(TiO_2)_1$	224.16	1.48	0.14	2.03
$Sn_{58.5}Al_{20}Sb_{15}Pb_5(TiO_2)_{1.5}$	230.94	1.97	0.14	1.62

Creep behavior

Creep behavior of $Sn_{80-x}Sb_{10}Pb_5(TiO_2)_x$ and $Sn_{60-x}Al_{20}Sb_{15}Pb_5(TiO_2)_x$ alloys were investigated by indentation method (Vickers hardness test) performed at room temperature. The indentation creep data are shown in Figure 9, where the indentation length is plotted against the indentation time applying constant load of 10 g. The indentation length increases with the indentation time. In the Mulheam-Tabor method, Figure 9, Vickers hardness number of $Sn_{80-x}Sb_{10}Pb_5(TiO_2)_x$ and $Sn_{60-x}Al_{20}Sb_{15}Pb_5(TiO_2)_x$ alloys are plotted versus indentation time on log-log scale for the indentation data. It is observed that there exists a linear relationship between indentation time and hardness for all conditions. The slope of the resultant lines according Mulheam-Tabor method is $-\left(n+\frac{1}{2}\right)$ where n is the stress exponent. The stress exponent values of $Sn_{80-x}Sb_{10}Pb_5(TiO_2)_x$ and $Sn_{60-x}Al_{20}Sb_{15}Pb_5(TiO_2)_x$ alloys are given in Table 7. These exponent values are in the range of 2.16 to 5.75 depending on the composition of used alloy and that agreed with the pervious results (n= 4.5 [19] and n ~ 5.3 to 5.6 and 5.8 to 5.9 [20]. The change in stress exponent values are attributable to microstructural features (changing in β matrix such as change in the lattice parameters, solid solution, size and distribution of strengthening phases, intermetallic phases) and that is agree with the pervious results [21].

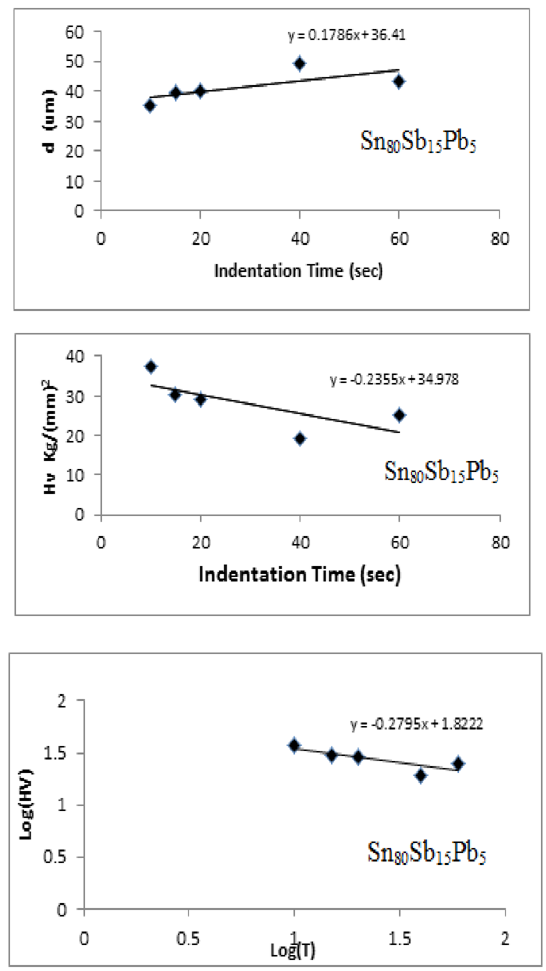

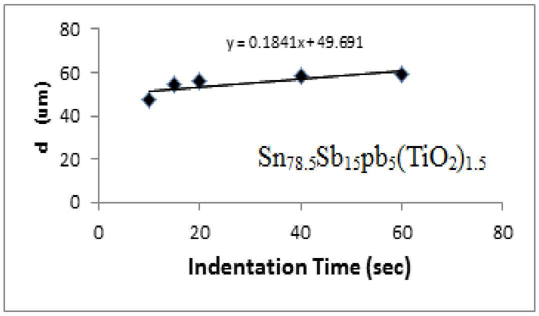

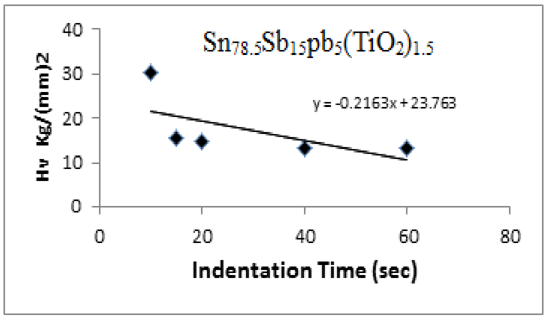

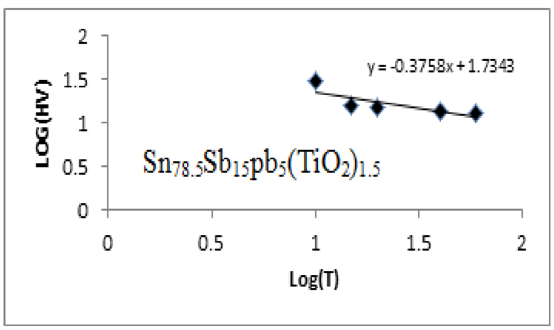

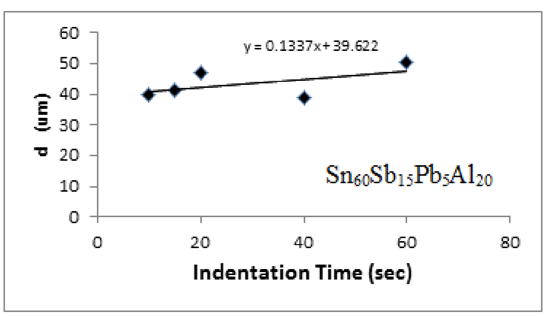

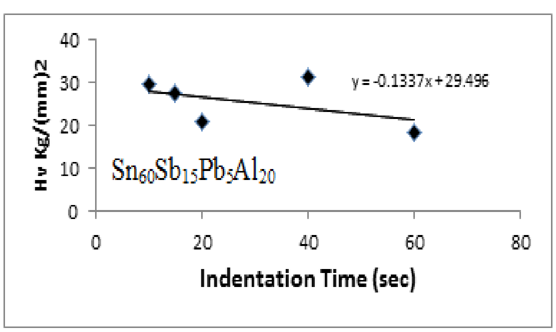

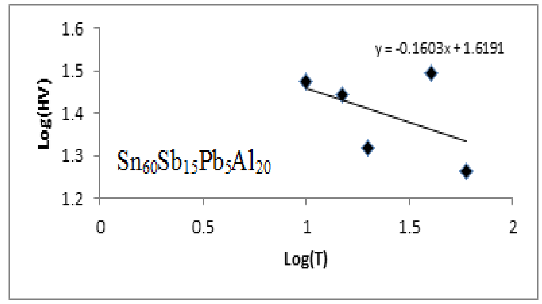

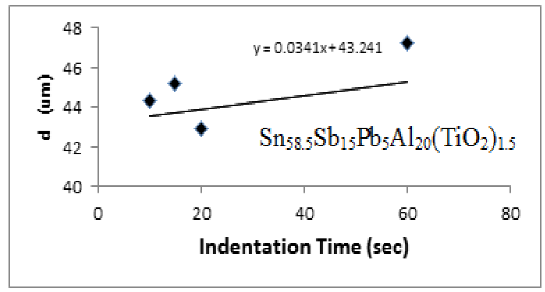

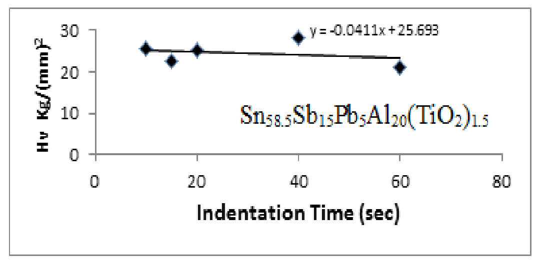

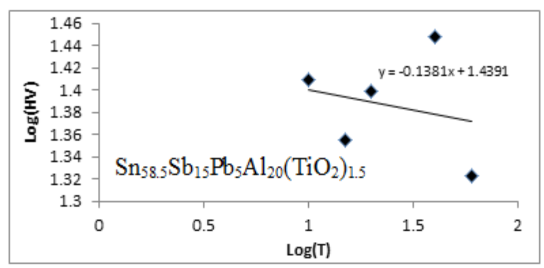

Figure 9:- indentation creep data of $Sn_{80-x}Sb_{10}Pb_5(TiO_2)_x$ and $Sn_{60-x}Al_{20}Sb_{15}Pb_5(TiO_2)_x$ alloys

Table 7:- stress exponent of and $Sn_{80-x}Sb_{10}Pb_5(TiO_2)_x$ $Sn_{60-x}Al_{20}Sb_{15}Pb_5(TiO_2)_x$ alloys

Samples	Stress exponent (n)
$Sn_{80}Sb_{15}Pb_5$	3.077
$Sn_{78.5}Sb_{15}Pb_5(TiO_2)_{1.5}$	2.16
Sn_{60} $Al_{20}Sb_{15}Pb_5$	5.749
$Sn_{58.5}$ $Al_{20}Sb_{15}Pb_5(TiO_2)_{1.5}$	2.44

5. CONCLUSIONS

Microstructure of tin- antimony- lead and tin- aluminum- antimony- lead alloys changed after adding titanium oxide. Stress exponent of tin- antimony- lead and tin- aluminum- antimony- lead alloys decreased after adding titanium oxide. Strengths of tin- antimony- lead and tin- aluminum- antimony- lead alloys increased after adding titanium oxide. Internal fiction and thermal parameters of tin- antimony- lead and tin- aluminum- antimony- lead alloys varied after adding titanium oxide. The $Sn_{79}Sb_{15}Pb_5(TiO_2)_1$ and $Sn_{59}Al_{20}Sb_{15}Pb_5(TiO_2)_1$ alloys have better bearing properties for industrial applications

6. REFERENCES

[1] Zeren A, Feyzullahoglu E, Zeren M, Mater. and Design 28 (2007) 318
[2] El-Bediwi A, Radiation Effects & Defects in Solids 159 (2004) 125
[3] El- Bediwi A, Cryst. Res. Technol 40: 7 (2005) 688
[4] El-Bediwi A, Radiation Effects & Defects in Solids 159 (2004) 539
[5] Mahmudi R, J. Mater. Sci. 40 (2005) 3361
[6] Mahmudi R and Rezaee-Bazzaz A, Mater. Lett. 59: 13 (2005) 1705
[7] Mahmudi R, Geranmay A.R, Bakher M, Allam M, Mater. Sci. and Eng. A 457 (2007) 173
[8] Esfandyarpour M.J, Mahmudi R, Mater. Sci. and Eng. A 530 (2011) 402
[9] El-Bediwi A, Lashin A.R, Mossa M, Kamal M, Mater. Sci. and Eng. A 528 (2011) 3568
[10] Goudarzi M.M, Jahromi S.A.J, Nazarboland A, Mater. and Design 30 (2009) 2283
[11] Kamal M, Abdel-Salam A, Pieri J.C, J. Mater. Sci 19 (1984) 3880
[12] El- Bediwi A.B, El Said Gouda, Kamal M, AMSE, 65, n° 1, Modeling C- 2004
[13] El-Daly A.A, Mohamad A.Z, Fawzy A, El-Taher A.M, Mater. Sci. and Eng. A 528 (2011) 1055
[14] Bora M.O, Coban O, Sinmazcelik T, Gunay V, Zeren M, Mater. and Design 31 (2010) 2707
[15] Xiaowu H, Shuangming L, Lin L, Hengzhi F, The Chinese Journal of Nonferrous Metals 14:1 (2004) 93
[16] Schreiber E, Anderson O. L and Soga N, Elastic constant and their measurements, McGraw-Hill, New York, (1973) 82
[17] Timoshenko S and Goddier J.N, "Theory of elasticity, 2nd Ed", McGraw-Hill, New York, (1951) 277
[18] Nuttall K, J. Inst. Met. 99 (1971) 266
[19] Geranmayeh A. R, Mahmudi R, J Matter Sci. 40 (2005) 3361
[20] Kangooie M, Mahmudi R and Geranmayeh A. R., J Electr. Matter. 39 (2010) 215
[21] Deraki Rani S, Murthy G. S, Mate. Sci. Techn., 403 (2004) 20